Journal of Hazardous Materials 183 (2010) 315–323

Contents lists available at ScienceDirect

Journal of Hazardous Materials

journal homepage: www.elsevier.com/locate/jhazmat

Ecofriendly synthesis and solar photocatalytic activity of S-doped ZnO

Ashokrao B. Patil[a], Kashinath R. Patil[b], Satish K. Pardeshi[a,*]

[a] Department of Chemistry, University of Pune, Ganeshkhind, Pune 411007, India
[b] Center for Materials Characterization, National Chemical Laboratory, Pune 411008, India

ARTICLE INFO

Article history:
Received 26 April 2010
Received in revised form 7 July 2010
Accepted 8 July 2010
Available online 15 July 2010

Keywords:
S-doped ZnO
XPS
Photoluminescence
Photocatalysis
Resorcinol
Sunlight

ABSTRACT

The S-doped ZnO was prepared by new ecofriendly method, which involves simple mechanochemical synthesis followed by thermal decomposition of bisthiourea zinc oxalate (BTZO) powders. The BTZO was characterized by FTIR and TG–DTA analysis while S-doped ZnO crystallite was characterized by XRD, XPS, SEM, EDXS, and photoluminescence (PL) spectra. X-ray diffraction data suggest the single phase wurtzite structure for S-doped ZnO and the incorporation of sulfur expand the lattice constants of ZnO. Room temperature PL spectra show more number of oxygen vacancies in S-doped ZnO as compare to that of pure ZnO. Photocatalytic activity of S-doped ZnO was checked by means of solar photocatalytic degradation (PCD) of resorcinol, using a batch photoreactor. The PCD efficiency of S-doped ZnO was found to be 2 times greater than that of pure ZnO. The inherent relationship between PL intensity and photocatalytic activity of S-doped ZnO was discussed.

© 2010 Elsevier B.V. All rights reserved.

1. Introduction

Semiconductor mediated photocatalysis is an efficient method for environmental detoxification [1–4], which is capable of converting the toxic and nonbiodegradable organic compounds into carbon dioxide and inorganic constituents. Among the various semiconductors applied, titanium dioxide is the most widely employed photocatalyst but it is effective only under irradiation of UV-light [5]. The photocatalytic degradation of organic contaminants using solar light could be highly economical compared with the processes using artificial UV radiation, which requires substantial amount of electrical power. In this regard, a photocatalyst with strong absorption in the visible region needs to be developed.

Zinc oxide is another important wide band gap semiconductor, which is bio-safe and biocompatible material and can be directly used in heterogeneous photocatalysis [6]. Basically ZnO exhibits more efficiency than TiO_2 in photocatalytic degradation of some dyes under visible light illumination [7]. In order to improve photocatalytic activity of ZnO in visible light, it is doped with nonmetal such as nitrogen [8], sulfur [9]. The sulfur doping in ZnO is expected to modify the optical, electrical and photocatalytic properties because of large electronegativity and size difference between S and O [10]. Doping sulfur is an efficient method for narrowing the band gap energy of semiconductor oxide and shifts the threshold wavelength to the visible light region [11]. This could be helpful to utilize solar energy for the elimination of organic hazards by photocatalysis. Chen et al. [9] observed that the nonmetal impurities (N, S, C) can interfere with the crystallization of ZnO which can improve photocatalytic activity by enhancing absorption of light and transport of photogenerated charge carriers. The S-doped ZnO have been synthesized by variety of methods such as chemical solution-conversion process [12], electrochemical deposition [13] and air oxidation of ZnS [14]. The mechanochemical doping is one of the convenient methods employed for the doping of nonmetal elements into metal oxides [8,15]. In most of the mechanochemical doping methods grinding operations are performed by zirconia/planetary ball mill. In present study we are reporting the ecofriendly synthesis of S-doped ZnO which involves solution free mechanochemical synthesis and simple thermal decomposition of bisthiourea zinc oxalate. The S-doped ZnO synthesized by this method shows better solar photocatalytic degradation (PCD) of resorcinol as compare to that of pure ZnO.

2. Experimental

2.1. Materials

In present study, zinc acetate (assay ≥ 98%), oxalic acid (assay 99.5%), thiourea (assay 99%), resorcinol (assay 99%) and other required chemicals are of analytical grade, obtained from Merck Limited, Mumbai, India and were used without further purification. The appropriate concentration of resorcinol solutions was prepared by using double distilled water.

* Corresponding author. Tel.: +91 020 25601394x514; fax: +91 020 25691728.
E-mail address: skpar@chem.unipune.ernet.in (S.K. Pardeshi).

0304-3894/$ – see front matter © 2010 Elsevier B.V. All rights reserved.
doi:10.1016/j.jhazmat.2010.07.026

$$Zn(CH_3COO)_2.2H_2O + H_2C_2O_4.2H_2O \xrightarrow{\text{Hand grinding}} Zn(C_2O_4).2H_2O + 2\,CH_3COOH + 2H_2O \quad (a)$$

$$Zn(C_2O_4).2H_2O + 2\,SC(NH_2)_2 \xrightarrow{\text{Hand grinding}} Zn[C_2O_4][SC(NH_2)_2]_2 + 2H_2O \quad (b)$$

Bisthiourea Zinc Oxalate

Scheme 1. Synthesis of bisthiourea zinc oxalate.

2.2. Synthesis of S-doped zinc oxide

Sulfur-doped zinc oxide was prepared by a novel two-step process. The first step is solution free mechanochemical synthesis of bisthiourea zinc oxalate (BTZO) powders and the second step is thermal decomposition of BTZO to form S-doped ZnO. In a typical synthesis, 219.5 mg of zinc acetate dihydrate and 151.2 mg of oxalic acid were taken in agate mortar and mixture was hand ground for 10 min at room temperature to obtain paste (semisolid) of zinc oxalate dihydrate and acetic acid by-product (Scheme 1a). Then 152.2 mg of thiourea was added and hand grinding process was continued for next 20 min. The thiourea coordinates with zinc oxalate to form bisthiourea zinc oxalate complex (Scheme 1b). After 1 h, most of the acetic acid by-product goes off from the reaction mixture and semisolid gradually turns into fine powder of BTZO. Finally, dark yellow colored S-doped ZnO was obtained by calcination of BTZO at 600 °C. Same procedure is repeated, without adding thiourea to obtain zinc oxalate (ZO) and pure ZnO for comparison.

2.3. Equipments

The BTZO was characterized by FTIR (Shimadzu FTIR-8400 spectrometer equipped with KBr beam splitter) and thermogravimetry (Shimadzu TG–DTG-60H). While, S-doped ZnO crystallite were characterized by X-ray diffractometer (D-8 Advance Brkur AXS), energy dispersive X-ray spectra (EDXS) attached to scanning electron micrograph (SEM JEOL JSM-6360A) and photoluminescence (PL) spectra (Shimadzu, RF-5301PC). X-ray photoelectron spectra (XPS) of S-doped ZnO were recorded with a V. G. Microtech (UK) unit ESCA 3000 spectrometer equipped with Mg Kα X-ray source ($h\upsilon$ = 1253.6 eV) and a hemispherical electron analyzer. The X-ray source was operated at 150 W. The residual pressure in the ion-pumped analysis chamber was maintained below 1.0×10^{-9} Torr during data acquisition. The C 1s peak at a binding energy 284.6 eV was taken as an internal standard. The accuracy of BE values was within ±0.2 eV. The photocatalytic reactions were carried out at ambient temperature under the irradiation of sunlight in batch photoreactor. The details of setup of photoreactor were already explained elsewhere [16]. The initial pH of suspension was recorded with the help of pH meter (EUTECH-pH510). The extent of photocatalytic degradation (PCD) at an interval of 1 h sunlight irradiation was primarily checked by means of decrease in absorbance on UV–vis spectrophotometer (UV-1601, Shimadzu). Complete mineralization of resorcinol was confirmed by chemical oxygen demand (COD) reduction method. The COD determination tests were performed according to standard dichromate method [17] using COD digester (SPECTRALAB 2015M). The photocatalytic degradation (PCD) efficiency was calculated from the following expression (1):

$$\eta = \frac{COD_i - COD_t}{COD_i} \times 100 \quad (1)$$

where η is the photocatalytic degradation efficiency, COD_i is the initial chemical oxygen demand, COD_t is the chemical oxygen demand at time t. The intensity of sunlight was periodically checked by ferrioxalate actinometry [18]. The average photon flux calculated for sunlight was found to be 1.7×10^{-7} Einstein s^{-1} cm^{-2}. The PCD intermediates were identified by HPLC and GC–MS analysis. HPLC analysis was performed with a Shimadzu 20A instrument equipped with C18 column. Acetonitrile/water (40:60) was used as mobile phase at a flow rate of 1 mL min^{-1}. The sample injection volume of 10 μL and UV wavelength of 254 nm were employed. GC–MS analysis was done with Shimadzu GCMS-QP5050 instrument equipped with DB-5 capillary column and Quadrapole detector. Helium was used as a carrier gas. The GC injection volume of 2 μL and the split ratio of 25:30 were used.

The reusability of the photocatalyst was evaluated by reclaiming the photocatalyst after PCD reaction in the batch mode, washing, drying in electric oven at 110 °C and using it for resorcinol degradation under similar experimental conditions.

2.4. Photocatalytic degradation experiments

The PCD efficiency of S-doped zinc oxide was investigated by means of solar photocatalytic degradation of resorcinol a model endocrine disruptor. All PCD experiments were carried out in duplicate and at an ambient temperature, without external supply of oxygen. Pure resorcinol (Merck, 99%) was dissolved in double distilled water to obtain desired concentration solutions. In all PCD experiments, 100 mL resorcinol solution (150 ppm) was taken in batch photocatalytic reactor vessel and optimum amount of photocatalyst was added and mixture was agitated in an ultrasonic bath for 5 min to obtain uniform suspension. Initial pH of suspension was recorded and whole setup was then placed in sunlight with constant stirring for specific period of time between 9:00 a.m. to 5:00 p.m. during the months of December to March. After the specific sunlight irradiation time PCD reaction was stopped and whole suspension was centrifuged at a speed of 3000 rpm for 5 min (Remi, India) and then filtered through a 0.45 μm polytetrafluro ethylene (PTFE) filter. The filtrate was directly used for absorbance and COD measurement. While, some part of filtrate was acidified with dil. H_2SO_4 and extracted with ethyl acetate. The resulting sample was then dried under vacuum and used for GC–MS analysis.

The extent of degradation of resorcinol was also studied under similar experimental conditions in the dark as a control experiment.

3. Results and discussion

3.1. Characterization of BTZO complex

Fig. 1 shows the FTIR spectrum of BTZO and ZO synthesized by mechanochemical method. The FTIR frequencies and assignment of bands of ZO and BTZO in the region 4000–400 cm^{-1} are summarized in Table 1. The high frequency N–H absorption bands in the region 3400–3100 cm^{-1} of the BTZO spectrum were not shifted to a lower frequency upon formation of metal thiourea complex, indicating that nitrogen to zinc bonds are absent and that the bonding must be between sulfur and zinc atoms [19]. There is distinct band at 2705 cm^{-1} in BTZO which corresponds to symmetric stretching modes of NH_2 groups of thiourea. Similar observation was reported by Dhumane et al. [20] for Zn $[CS(NH_2)_2]_2Cl_2$ complex, stating that there is bonding between sulfur and zinc.

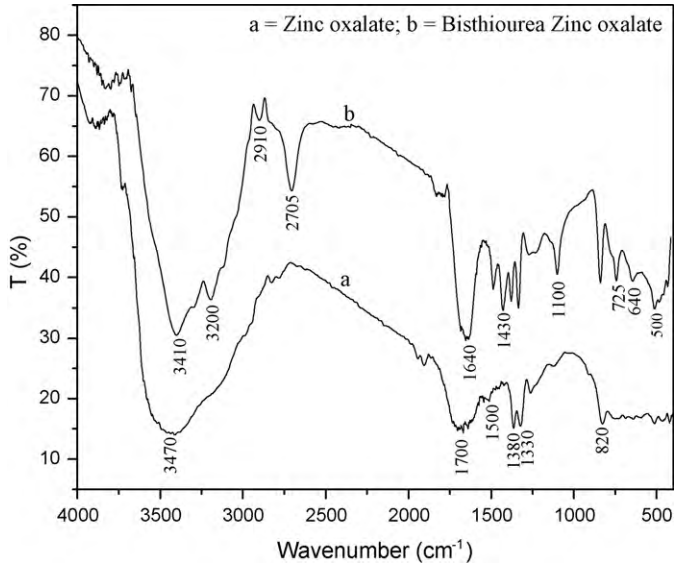

Fig. 1. FTIR spectra of bisthiourea zinc oxalate and zinc oxalate dihydrate.

Table 1
Infrared spectral data of BTZO and ZO.

FTIR bands common in BTZO and ZO		Exclusive FTIR bands of BTZO	
Wave number (cm^{-1})	Assignment	Wave number (cm^{-1})	Assignment
1700 s	υ_s C=O stretch	3410 vs	υ_{as} N–H stretch
1380 m	υ_s C–O stretch	3200 m	υ_s N–H stretch
1330 m	υ_s C–O stretch	2910 w	υ_s C–C stretch
820 sh	υ_s O–C–O def	2705 sh	υ_s NH_2 stretch
		1670–1640 vs	δ NH_2
		1430 sh	υ_{as} C–S
		1100 sh	υ_s C–N
		725 m	υ_s C–S
		640 w	t NH_2
		500 m	δ_s S–C–N def

The thermal behavior of BTZO complex has been studied by means of TG–DTA–DTG presented in Fig. 2. The thermal decomposition process of BTZO is complicated and produces several endo- and exothermal effects. There are three major weight loss processes from 30 °C to 600 °C in TG. The 12% weight loss from 30 °C to 150 °C was assigned to the loss of adsorbed water and release of remaining acetic acid by-product. The acetic acid molecules easily volatilized into air during the process of hand grinding. However, it has a boiling point of 118 °C, so the remaining acetic acid can only be totally removed at a temperature higher than its boiling point. The endothermic effect at 120 °C registered on DTA was assigned to the dehydration and removal of acetic acid while that at 210 °C was attributed to the melting of BTZO. The 17% weight loss observed from 150 °C to 225 °C was attributed to decomposition of thiourea molecules coordinated with Zn into CS_2, HNCS and NH_3 [21]. The 36% weight loss observed from 225 °C to 450 °C in TG curve is due to decomposition of oxalate moiety of BTZO to form zinc sulfide. This is seen in terms of broad exothermic peak in DTA at this temperature range. The ZnS is unstable in air at higher temperature and undergoes air oxidation to form ZnO; this shows gradual weight loss of 6.5% from 450 °C to 600 °C in TG curve. During this conversion there is incorporation of S into ZnO. The DTG curve shows three major peaks centered at 97 °C, 243 °C and 425 °C corresponding to the weight losses in TG curve. The observed weight loss of 71.5% was very close to that of calculated values (73.4%) and matches to $Zn[C_2O_4][SC(NH_2)_2]_2$ formula (structure 1) for BTZO.

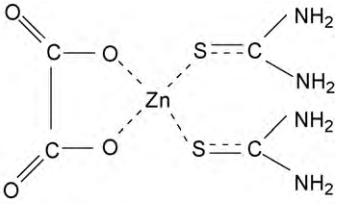

Structure 1

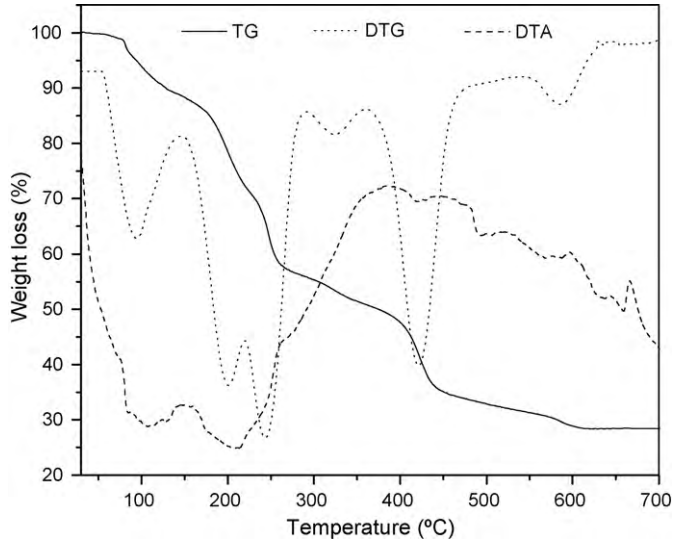

Fig. 2. TGA–DTA analysis of bisthiourea zinc oxalate.

3.2. Characterization of S-doped ZnO

The BTZO complex was calcined to obtain S-doped ZnO and characterized by various techniques.

3.2.1. XRD analysis of S-doped ZnO

Fig. 3 illustrates the XRD pattern of stepwise formation of S-doped ZnO from BTZO complex. The XRD pattern of powders obtained by calcination of BTZO at 450 °C and 500 °C shows peaks at $2\theta = 28.8°$ (1 1 1), 47.7° (2 2 0), 56.5° (3 1 1), 76.9° (3 3 1) which exactly matches XRD data of JCPDS card No. 5-0566, for ZnS sphalerite cubic phase ($a = 5.3926$ Å) and that of pure commercial ZnS (Sigma–Aldrich, 99.99%) (Fig. 3a–c). When the BTZO calcined at 550 °C, intensity of 28.8° (1 1 1) peak was found to be decreased and five peaks are newly appeared at $2\theta = 31.7°$ (1 0 0), 34.3° (0 0 2), 36.2° (1 0 1), 62.7° (1 0 3) and 67.9° (1 1 2) (Fig. 3d). New diffraction peaks can be indexed for hexagonal wurtzite structure of ZnO ($a = 3.249$ Å; $c = 5.206$ Å) and diffraction data were in good agreement with the JCPDS card 36-1451 for ZnO. When BTZO calcined at 600 °C all the characteristic peaks of ZnS disappeared with simultaneous development of complete XRD pattern of ZnO (Fig. 3e). This indicates that when BTZO is calcined from 450 °C to 550 °C it forms ZnS, which is further oxidized into the ZnO from 550 °C to 600 °C. The XRD pattern of BTZO calcined at 600 °C (Fig. 3e) was broader than that of pure ZnO obtained by calcination of zinc oxalate at 600 °C (Fig. 3f). The broadening of XRD peaks indicates that there is incorporation of S into the ZnO when BTZO was calcined at 600 °C. The successful doping of S in ZnO was supported by lower Bragg angle shift (by 0.18°) in XRD pattern of S-doped ZnO as compare to that of pure ZnO. The lower Bragg angle shift of (1 0 1) peak is shown separately in Fig. 3.

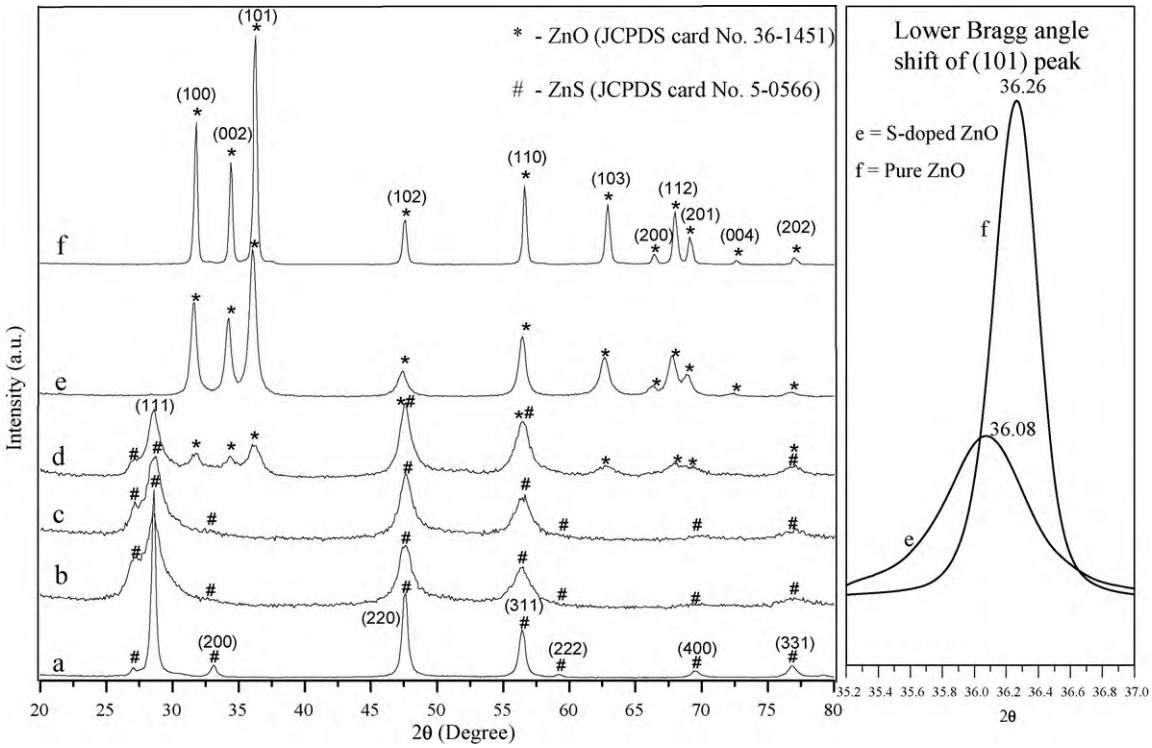

Fig. 3. XRD pattern of S-doped ZnO obtained by calcination of bisthiourea zinc oxalate, (a) commercial ZnS; bisthiourea zinc oxalate calcined at (b) 450 °C; (c) 500 °C; (d) 550 °C; (e) 600 °C (S-doped ZnO) and (f) zinc oxalate calcined at 600 °C (pure ZnO).

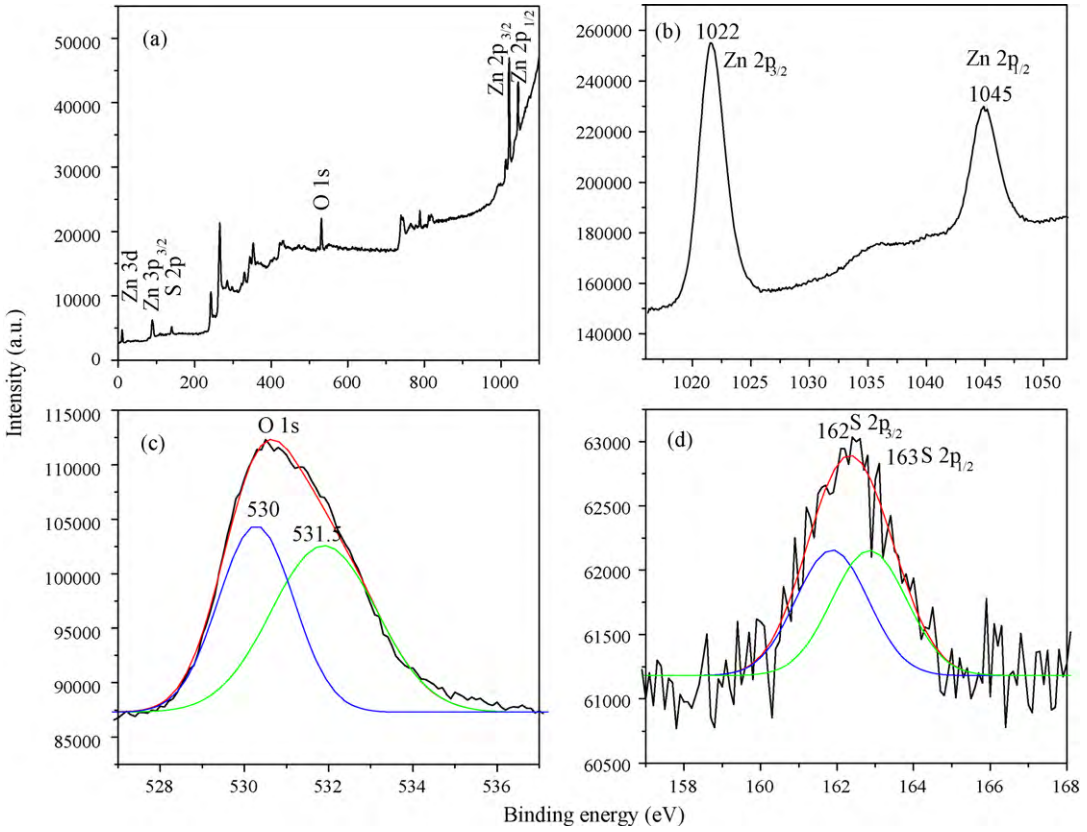

Fig. 4. XPS whole scanning spectrum (a); fine spectra of Zn $2p_{3/2}$, Zn $2p_{1/2}$ (b); O 1s (c); and S $2p_{1/2}$ (d) of S-doped ZnO.

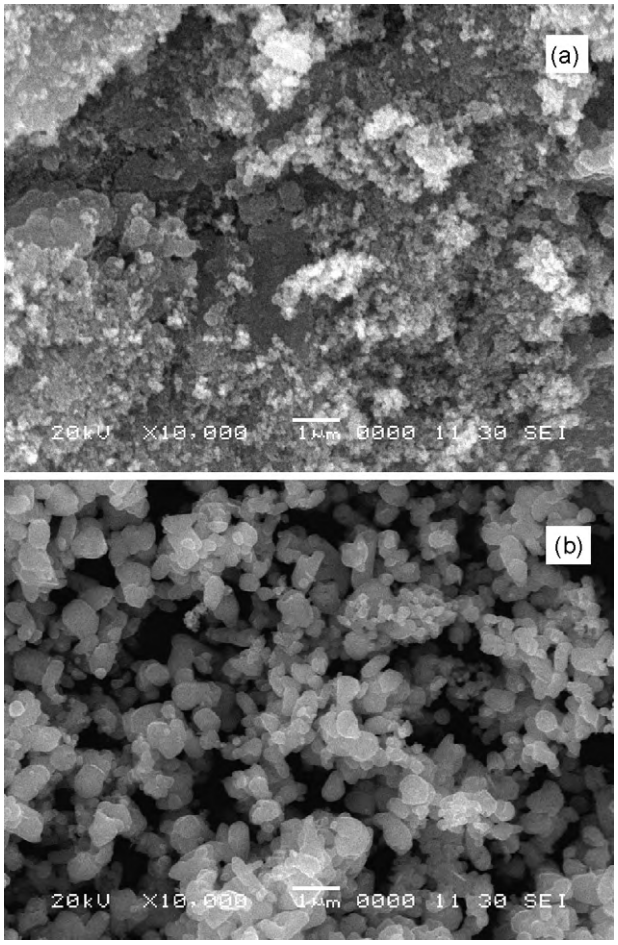

Fig. 5. SEM of Bisthiourea zinc oxalate calcined at (a) 550 °C and (b) 600 °C (S-doped ZnO).

3.2.2. XPS analysis of S-doped ZnO

The composition of S-doped ZnO was determined by XPS analysis. Fig. 4a shows the whole scanning spectrum of S-doped ZnO. The peaks located at 1022 eV and 1045 eV are assigned to electronic states of Zn $2p_{3/2}$ and Zn $2p_{1/2}$ respectively (Fig. 4b). Fig. 4c shows O 1s XPS spectrum, the peak at 530 eV was attributed to O^{2-} ions of ZnO, while another at 531.5 eV is usually associated with the adsorbed O_2 [13]. In Fig. 4d, the peaks positioned at 162 eV and 163 eV are assigned to the S $2p_{3/2}$ and S $2p_{1/2}$ electronic states respectively. Thus the XPS data supports the incorporation of S into the ZnO.

3.2.3. SEM–EDXS analysis

The SEM pictures of BTZO calcined at 550 °C and 600 °C are shown in Fig. 5. At 550 °C there are two distinct phases of ZnS and ZnO which clearly shows heterogeneous morphology with agglomeration (Fig. 5a). On the other hand the single homogeneous phase of S-doped ZnO was observed at 600 °C (Fig. 5b), which indicates the uniform doping of S into ZnO. Energy dispersive X-ray spectrum (EDXS) of S-doped ZnO is shown in Fig. 6. It shows peaks corresponding to Zn, O and S. No trace amount of other impurities could be seen in the detection limit of the EDXS which also supports the doping of sulfur in ZnO.

3.2.4. Optical properties of S-doped ZnO

The PL spectra of S-doped ZnO and pure ZnO obtained by calcination of BTZO and ZO, respectively, at 600 °C with excitation wavelength of 300 nm are shown in Fig. 7. The pure and S-doped

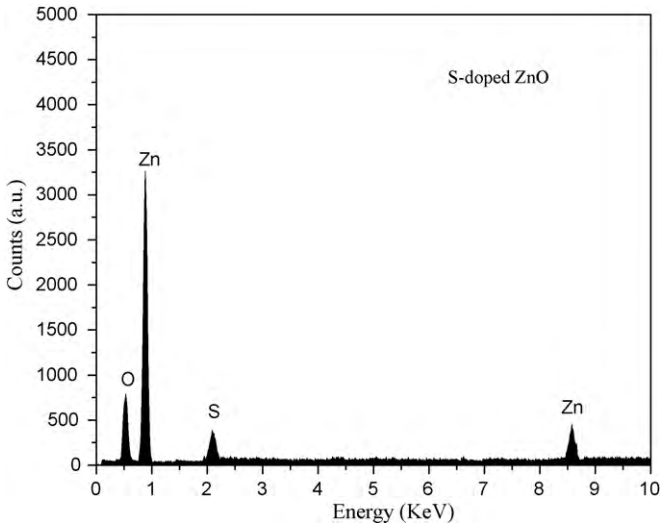

Fig. 6. Energy dispersive X-ray spectra of S-doped ZnO.

ZnO samples exhibit relatively weak UV emission band at about 390 nm and 370 nm, respectively, corresponds to the near band edge (NBE) emission, which is responsible for the recombination of the free excitons of ZnO. It is well known that the green yellow emission band at 507 nm originates from deep level (DL) defect emission associated with oxygen vacancies in ZnO lattices. Larger the content of oxygen vacancy or defect, stronger is the PL signal [22]. The green emission band of S-doped ZnO (Fig. 7a) was found to be 1.5 times stronger than that of pure ZnO (Fig. 7b) which indicates that large number of oxygen vacancies exists in S-doped ZnO.

3.3. Photocatalytic activity of S-doped ZnO

We selected resorcinol as a model organic pollutant for the study of PCD efficiency of S-doped ZnO because it is endocrine disrupting chemical.

3.3.1. Effect of the initial concentration of resorcinol

The PCD of resorcinol over S-doped ZnO at different initial concentrations in the range 50–300 ppm was investigated as a function of sunlight irradiation time at the natural pH of suspension (without adjustment). The PCD efficiency is measured in terms of decrease in

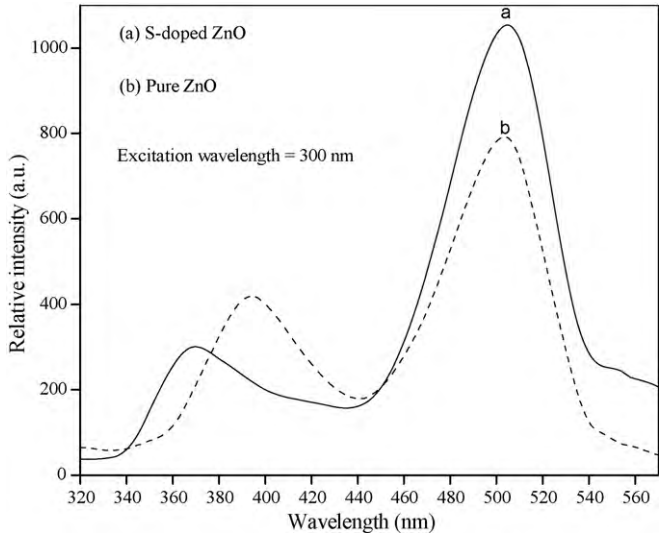

Fig. 7. Photoluminescence spectra of S-doped ZnO and pure ZnO (λ_{ex} = 300 nm).

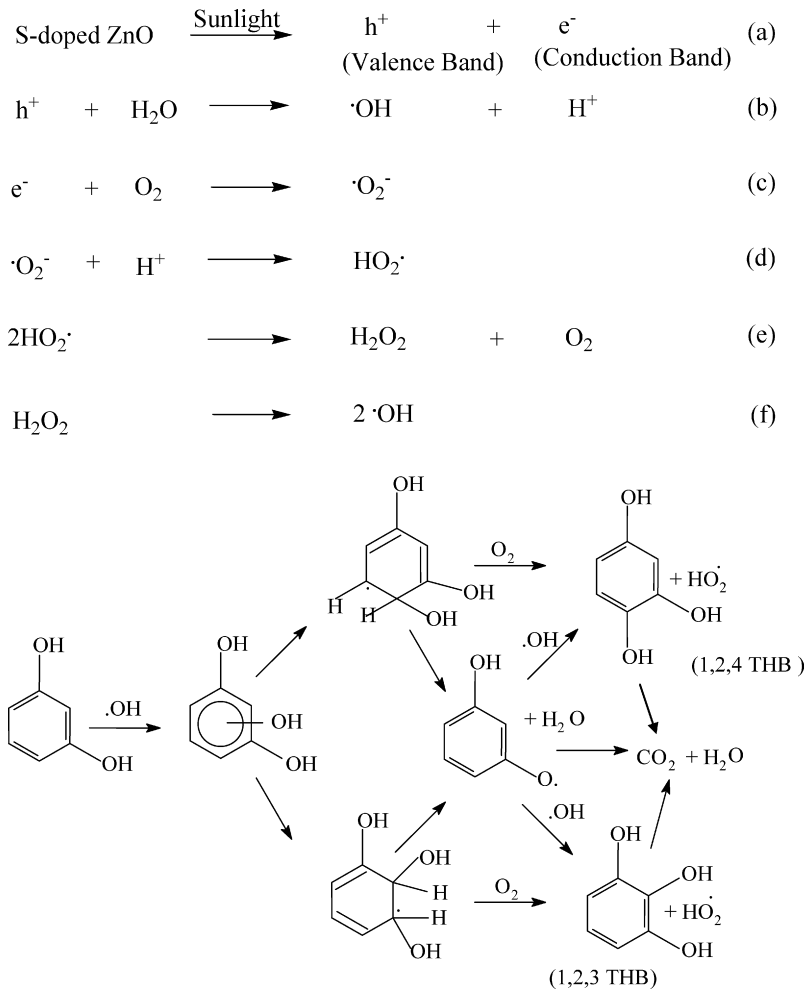

Scheme 2. Photocatalytic degradation of resorcinol over S-doped ZnO.

COD of resorcinol and results are illustrated in Fig. 8. The 150 ppm resorcinol was completely mineralized by using 250 mg/100 mL of S-doped ZnO and it shows approximately double PCD efficiency than that of pure ZnO. However after 150 ppm, PCD efficiency was found to be inversely affected by concentration of resorcinol. As the concentration of resorcinol increases, the photons get interrupted before they can reach the photocatalyst surface hence absorption of photons by the photocatalyst decreases and consequently the PCD was reduced. The PCD efficiency of S-doped ZnO was found to be greater than that of pure ZnO. This could be correlated with more number of oxygen vacancies in S-doped ZnO than that of pure ZnO as seen in PL spectra of these materials (Fig. 7a and b). During the process of photocatalytic reaction, oxygen vacancies and defects become centers to capture photo-induced electrons, as a result the recombination of photo-induced electrons and holes can be effectively inhibited. Moreover, oxygen vacancies also promote the adsorption of O_2 which is converted into superoxide radicals ($^{\bullet}O_2^-$) by interacting with photo-induced electron (Scheme 2a–c). These $^{\bullet}O_2^-$ radicals are active to promote the oxidation of organic substances by forming other radicals such as $^{\bullet}OH$, $HO_2^{\bullet}$ (Scheme 2d–f). Thus, oxygen vacancies and defects are in favor of photocatalytic reactions and larger the content of oxygen vacancy or defect, higher is the photocatalytic activity. This shows that S-doped ZnO is effective photocatalyst in solar light as compare to pure ZnO. The 150 ppm resorcinol was selected as optimum concentration for the study of other parameters.

3.3.2. *Effect of photocatalyst loading*

The blank experiments were carried out without photocatalyst to examine the extent of resorcinol 'photolyzed' in the absence of photocatalyst. No detectable PCD of resorcinol was evidenced in aqueous solution in the absence of photocatalyst. When 150 ppm resorcinol containing photocatalyst was irradiated with sunlight, PCD of resorcinol was observed. Fig. 9 shows degradation profile of 150 ppm resorcinol under loadings of photocatalyst from 100 to 350 mg/100 mL. The PCD efficiency was gradually increased up to 250 mg/100 mL and then it was decreased. At lower photocatalyst loading level than the optimum amount, photonic absorption controls the efficiency of PCD due to limited surface area of photocatalyst. The increase in the amount of photocatalyst also increased the number of active sites on the photocatalyst surface, which in turn increased the number of hydroxyl, and superoxide radicals. Therefore efficiency of PCD increased linearly with increase in photocatalyst loading up to 250 mg. It is interesting to note that for every photocatalyst loading the PCD efficiency of S-doped ZnO was found to be approximately 2 times greater than that of pure ZnO. This is due to fact that the S doping into the ZnO introduces nonradiative relaxation pathway as well as increases surface to volume ratio in ZnO that enhances visible light absorption. The same observation was reported by Foreman et al. [23]. The S doping also interfere with the crystallization of ZnO and helps to absorb more photons and transport of the photogenerated charge carriers which improves PCD efficiency of S-doped ZnO. Above 250 mg

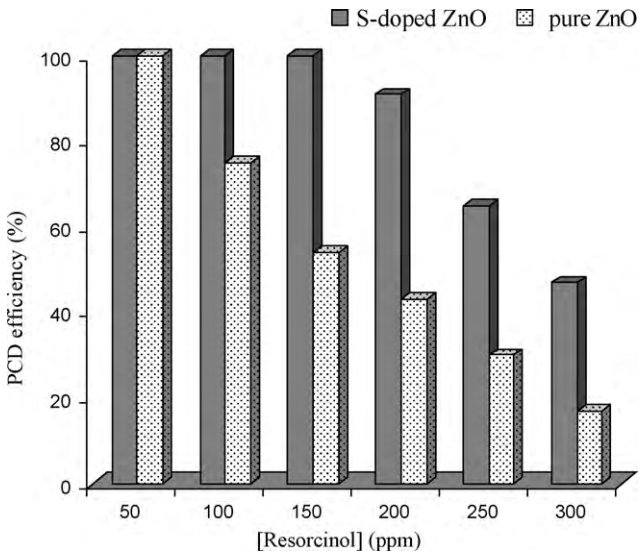

Fig. 8. Effect of concentration of resorcinol on PCD efficiency of S-doped ZnO. [Photocatalyst] = 250 mg/100 mL; initial pH of suspension = natural (6.7); intensity of sunlight = 1.7×10^{-7} Einstein s^{-1} cm^{-2}.

PCD efficiency declined with increasing photocatalyst loading. This could be attributed to shadowing effect, wherein the high turbidity due to high photocatalyst loading decreased the penetration depth of solar radiation. Hence, the optimal photocatalyst loading of 250 mg/100 mL was employed throughout the present study.

3.3.3. Effect of initial pH of the suspension

The effect of initial pH of suspension on PCD efficiency was studied from 4 to 10 with 150 ppm resorcinol solution and 250 mg/100 mL photocatalyst loading. The pH of the suspension was adjusted before irradiation of sunlight and it was not controlled during the course of reaction. All other parameters were kept constant. It is well known that in the acidic medium pure ZnO shows lower PCD efficiency due to slight (<1%) dissolution [24]. The S-doped ZnO shows greater PCD efficiency than the pure ZnO (Fig. 10) which indicates that it undergoes negligible dissolution in acidic

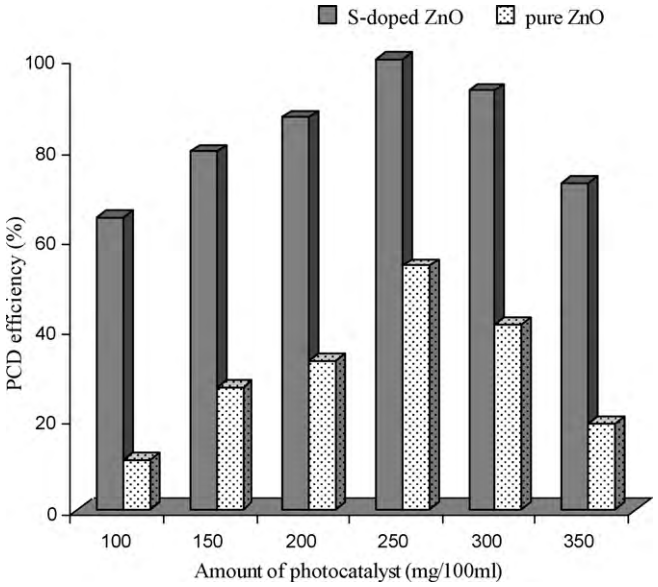

Fig. 9. Effect of amount of photocatalyst on PCD efficiency of S-doped ZnO. [Resorcinol] = 150 ppm; initial COD (COD_i) = 278 ppm; initial pH of suspension = natural (6.7); intensity of sunlight = 1.7×10^{-7} Einstein s^{-1} cm^{-2}.

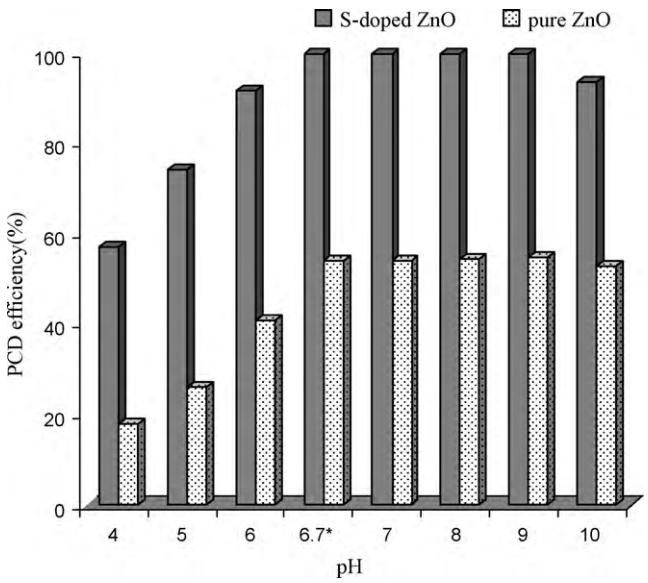

Fig. 10. Effect of pH on PCD efficiency of S-doped ZnO. [Resorcinol] = 150 ppm; initial COD (COD_i) = 278 ppm; [photocatalyst] = 250 mg/100 mL; intensity of sunlight = 1.7×10^{-7} Einstein s^{-1} cm^{-2}. *Natural pH of suspension (without adjustment).

medium. The extent of PCD of resorcinol was found to increase with increase in initial pH of suspension exhibiting better PCD in the neutral and alkaline pH. In alkaline medium, excess of hydroxyl anions facilitate photogeneration of •OH radicals which are accepted as primary oxidizing species responsible for PCD [25]. The natural pH (without adjustment) of 150 ppm resorcinol is 6.7. This solution was completely mineralized over S-doped ZnO; therefore other parameters were studied at natural pH of 150 ppm resorcinol.

3.3.4. Effect of irradiation time

The PCD efficiency of S-doped ZnO and pure ZnO in sunlight was found to increase with increase in irradiation time (Fig. 11). When 150 ppm resorcinol solution along with photocatalyst was magnetically stirred for 7 h in the absence of light (dark), negligible (5%) degradation was observed. For reference it is considered as zero hour irradiation. After 7 h irradiation of sunlight resorcinol solu-

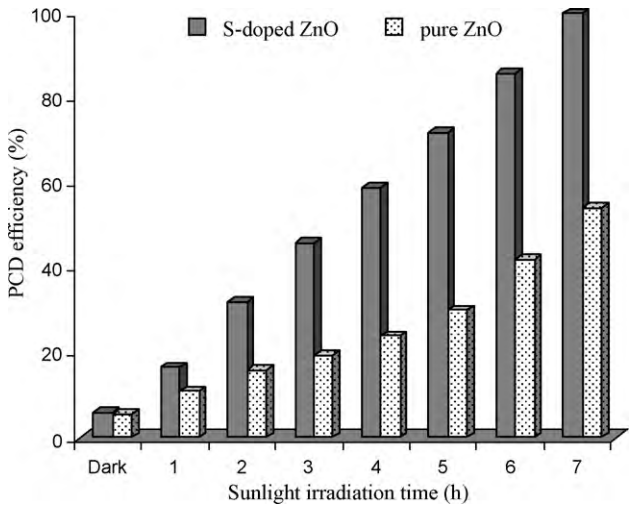

Fig. 11. Effect of sunlight irradiation time on PCD efficiency of S-doped ZnO. [Resorcinol] = 150 ppm; initial COD (COD_i) = 278 ppm; [photocatalyst] = 250 mg/100 mL; initial pH of the suspension = natural (6.7); intensity of sunlight = 1.7×10^{-7} Einstein s^{-1} cm^{-2}.

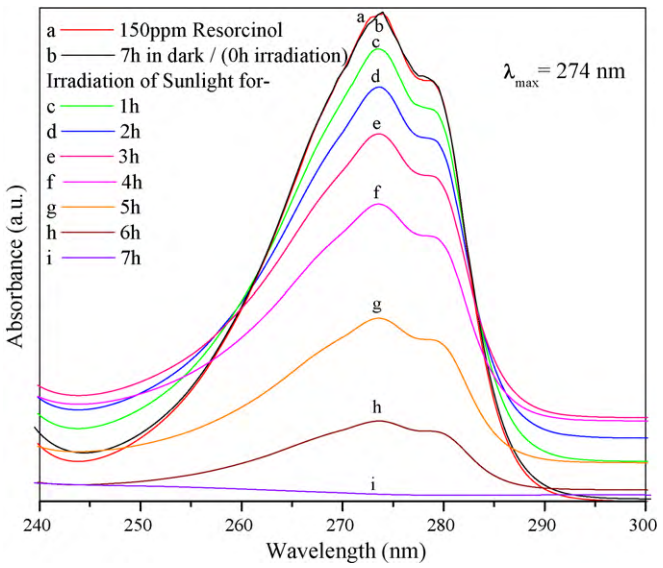

Fig. 12. UV–vis spectra showing photocatalytic degradation of resorcinol. [Resorcinol] = 150 ppm; initial COD (COD_i) = 278 ppm; initial pH of the suspension = natural (6.7); [S-doped ZnO] = 250 mg/100 ml; intensity of sunlight = 1.7×10^{-7} Einstein s^{-1} cm^{-2}.

tions of 150 ppm were completely mineralized over S-doped ZnO. It is observed that with increase in irradiation time, the absorbance of resorcinol at 274 nm (λ_{max}) was found to decrease and it becomes nearly zero after 7 h irradiation of sunlight (Fig. 12a–i). Thus 7 h irradiation time was selected for the study of other parameters. Fig. 13 shows a plot of ln (COD_i/COD_t) versus irradiation time for PCD of resorcinol over S-doped ZnO and bare ZnO. The linearity of kinetic curves reveals that the photocatalytic degradation of resorcinol follows apparent first order reaction kinetics. The apparent rate constants of PCD of resorcinol over S-doped ZnO are greater (2.51×10^{-1} h^{-1}) than that over pure ZnO (8.09×10^{-2} h^{-1}). Thus, the photocatalytic activity of S-doped ZnO determined in terms of the rate constant was found to be higher than that of bare ZnO.

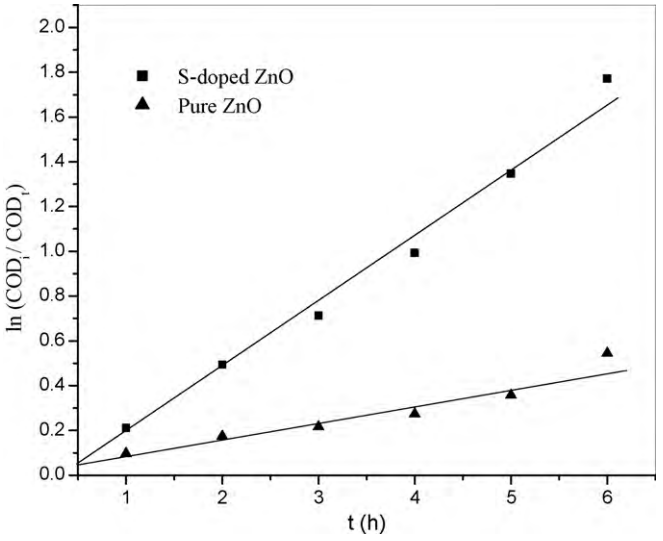

Fig. 13. Apparent first order linear transform ln (COD_i/COD_t) = $f(t)$ of the kinetic curves of resorcinol degradation over S-doped ZnO and pure ZnO.

3.4. Photocatalytic degradation mechanism

When optimum amount of S-doped ZnO was added to clear, aqueous solution of resorcinol (50–150 ppm) and agitated in an ultrasonic bath for 5 min, uniform milky white suspension was appeared. The white suspension was gradually masked to brown coloration when it was irradiated with sunlight because of formation of colored intermediates such as trihydroxy benzenes (THBs) [16]. The intensity of brown color was increased up to 4 h irradiation of sunlight. From 4 h to 7 h, the intensity of brown color was decreased as intermediates are converted in to CO_2 and H_2O. After 7 h irradiation of sunlight brown color was completely disappeared (milky white suspension was reappeared). When resorcinol molecules are adsorbed on the surface of S-doped ZnO particle, there is activation of these molecules by reaction with •OH radical, formed during photoexcitation of S-doped ZnO. The hydroxyl radical shows electrophilic character and prefer to attack electron rich ortho or para carbon atoms of resorcinol. It forms trihydroxycyclohexadienyl (TCHD) radicals that undergo further reaction with dissolved oxygen to yield THBs, with simultaneous generation of HO_2• radical. TCHD radicals are also converted to 3-hydroxyl phenoxy radical as shown in Scheme 2. The existence of 1,2,3-THB and 1,2,4-THB was confirmed by GC/MS and HPLC analysis. The further attack of •OH radical on TCHD and THB undergoes ring opening to form CO_2 and H_2O as a PCD products (Scheme 2).

4. Reuse of photocatalyst

The reuse of S-doped ZnO was separately studied, by keeping all other parameters constant. During this study, after sunlight irradiation for 7 h, photoreaction mixture was centrifuged and filtered. Filtrate was used for COD determination and residue was washed several times with double distilled water in ultrasonic bath followed by filtration and drying at 110 °C in an electric oven. Recovered S-doped ZnO was then reused for new PCD batch, without any further treatment such as heating in any kind of furnace. Activity of recycled S-doped ZnO was found to retain even after fifth photodegradation experiment.

5. Conclusions

In present study S-doped ZnO was synthesized by ecofriendly mechanochemical method. When bisthiourea zinc oxalate was calcined at 600 °C it forms S-doped ZnO, as confirmed by XRD, XPS, SEM, EDXS, and PL studies. The incorporation of S into ZnO was supported by broadening and lower Bragg angle shift (by 0.18°) in XRD pattern of S-doped ZnO as compare to that of pure ZnO. The XPS of S-doped ZnO shows the peaks positioned at 162 eV and 163 eV which are assigned to S $2p_{3/2}$ and S $2p_{1/2}$ electronic states respectively. The green emission band in room temperature PL spectra of S-doped ZnO was found to be 1.5 times stronger than that of pure ZnO which suggest that the large number of oxygen vacancies exist in S-doped ZnO. The oxygen vacancies and defects are in favor of photocatalytic reactions. The complete PCD of 150 ppm resorcinol was achieved over 250 mg/100 mL loading of S-doped ZnO at its natural pH within 7 h irradiation of sunlight. The rate constants of PCD of resorcinol over S-doped ZnO are greater (2.51×10^{-1} h^{-1}) than that over pure ZnO (8.09×10^{-2} h^{-1}). Hence, the solar PCD efficiency of S-doped ZnO was found to be 2 times greater than that of pure ZnO. Activity of recycled S-doped ZnO was found to retain even after fifth PCD experiment.

References

[1] T. Ohno, K. Tokieda, S. Higashida, M. Matsumura, Synergism between rutile and anatase TiO_2 particles in photocatalytic oxidation of naphthalene, Appl. Catal. A: Gen. 244 (2003) 383–391.

[2] S.K. Pardeshi, A.B. Patil, A simple route for photocatalytic degradation of phenol in aqueous zinc oxide suspension using solar energy, Solar Energy 82 (2008) 700–705.
[3] K. Chiang, T.M. Lim, L. Tsen, C.C. Lee, Photocatalytic degradation and mineralization of bisphenol A by TiO_2 and platinized TiO_2, Appl. Catal. A: Gen. 261 (2004) 225–237.
[4] H. Lachheb, E. Puzenat, A. Houas, M. Ksibi, E. Elaloui, C. Guillard, J.M. Herrmann, Photocatalytic degradation of various types of dyes (Alizarin S, Crocein Orange G, Methyl Red, Congo Red, Methylene Blue) in water by UV-irradiated titania, Appl. Catal. B: Environ. 39 (2002) 75–90.
[5] P. Qu, J. Zhao, T. Shen, H. Hidaka, TiO_2-assisted photodegradation of dyes: a study of two competitive primary processes in the degradation of RB in an aqueous TiO_2 colloidal solution, J. Mol. Catal. A: Chem. 129 (1998) 257–268.
[6] S.K. Pardeshi, A.B. Patil, Effect of morphology and crystallite size on solar photocatalytic activity of zinc oxide synthesized by solution free mechanochemical method, J. Mol. Catal. A: Chem. 308 (2009) 32–40.
[7] F. Peng, H. Wang, H. Yu, S. Chen, Preparation of aluminum foil-supported nanosized ZnO thin films and its photocatalytic degradation to phenol under visible light irradiation, Mater. Res. Bull. 41 (2006) 2123–2129.
[8] J. Lu, Q. Zhang, J. Wang, F. Saito, M. Uchida, Synthesis of N-doped ZnO by grinding and subsequent heating ZnO–urea mixture, Powder Technol. 162 (2006) 33–37.
[9] L.C. Chen, Y.J. Tu, Y.S. W, R.S. Kan, C.M. Huang, Characterization and photoreactivity of N-, S-, and C-doped ZnO under UV and visible light illumination, J, Photochem. Photobiol. A: Chem. 199 (2008) 170–178.
[10] G. Shen, J.H. Cho, J.K. Yoo, G.C. Yi, C.J. Lee, Synthesis and optical properties of S-doped ZnO nanostructures: nanonails and nanowires, J. Phys. Chem. B 109 (2005) 5491–5496.
[11] T. Ohno, M. Akiyoshi, T. Umebaysshi, K. Asai, T. Mitsui, M. Matsumura, Preparation of S-doped TiO_2 photocatalysts and their photocatalytic activities under visible light, Appl. Catal. A: Gen. 265 (2004) 115–121.
[12] G. Shen, J.H. Cho, S.I. Jung, C.J. Lee, Synthesis and characterization of S-doped ZnO nanowires produced by a simple solution-conversion process, Chem. Phys. Lett. 401 (2005) 529–533.
[13] X.H. Wang, S. Liu, P. Chang, Y. Tang, Influence of *S* incorporation on the luminescence property of ZnO nanowires by electrochemical deposition, Phys. Lett. A 372 (2008) 2900–2903.
[14] P. Zhou, X. Yu, L. Yang, Z. Tao, Simple air oxidation synthesis and optical properties of S-doped ZnO microspheres, Mater. Lett. 61 (2007) 3870–3872.
[15] Q.W. Zhang, J. Wang, S. Yin, T. Sato, F. Saito, Synthesis of a visible-light active $TiO_{2-x}S_x$ photocatalyst by means of mechanochemical doping, J. Am. Ceram. Soc. 87 (6) (2004) 1161–1163.
[16] S.K. Pardeshi, A.B. Patil, Solar photocatalytic degradation of resorcinol a model endocrine disrupter in water using zinc oxide, J. Hazard. Mater. 163 (2009) 403–409.
[17] J.T. Bellaire, G.A. Parr-Smith, Standard Methods for the Examination of Water and Wastewater, seventeenth ed., Am. Public Health Association, Washington, DC, 1985.
[18] C.G. Hatchard, C.A. Parker, A new sensitive chemical actinometer. II. Potassium ferrioxalate as a standard chemical actinometer, Proc. R. Soc. London A235 (1956) 518.
[19] K. Nakamoto, Infrared and Raman Spectra of Inorganic and Coordination Compounds, fourth ed., J. Wiley and Sons, New York, 1986, p. 269.
[20] N.R. Dhumane, S.S. Hussaini, V.V. Nawarkhele, M.D. Shirsat, Dielectric studies of metal complexes of thiourea crystals for electro-optic modulation, Cryst. Res. Technol. 41 (9) (2006) 897–901.
[21] S. Wang, Q. Gao, J. Wang, Thermodynamic analysis of decomposition of thiourea and thiourea oxides, J. Phys. Chem. B 109 (2005) 17281–17289.
[22] J. Liqiang, Q. Yichun, W. Baiqi, L. Shudan, J. Baojiang, Y. Libin, F. Wei, F. Honggang, S. Jiazhong, Review of photoluminescence performance of nano-sized semiconductor materials and its relationships with photocatalytic activity, Sol. Energy Mater. Sol. Cells 90 (2006) 1773–1787.
[23] J.V. Foreman, J. Li, H. Peng, S. Choi, H.O. Everitt, J. Liu, Time-resolved investigation of bright visible wavelength luminescence from sulfur-doped ZnO nanowires and micropowders, Nano Letters 6 (2006) 1126–1130.
[24] M.A. Behnajady, N. Modirshahla, R. Hamzavi, Kinetic study on photocatalytic degradation of C.I. acid yellow 23 by ZnO photocatalyst, J. Hazard. Mater. 133 (2006) 226–232.
[25] M. Muruganandham, M. Swaminathan, Solar photocatalytic degradation of a reactive azo dye in TiO_2-suspension, Sol. Energy Mater. Sol. Cells 81 (2004) 439–457.